

# NJC

Accepted Manuscript



This is an *Accepted Manuscript*, which has been through the Royal Society of Chemistry peer review process and has been accepted for publication.

*Accepted Manuscripts* are published online shortly after acceptance, before technical editing, formatting and proof reading. Using this free service, authors can make their results available to the community, in citable form, before we publish the edited article. We will replace this *Accepted Manuscript* with the edited and formatted *Advance Article* as soon as it is available.

You can find more information about *Accepted Manuscripts* in the [Information for Authors](#).

Please note that technical editing may introduce minor changes to the text and/or graphics, which may alter content. The journal's standard [Terms & Conditions](#) and the [Ethical guidelines](#) still apply. In no event shall the Royal Society of Chemistry be held responsible for any errors or omissions in this *Accepted Manuscript* or any consequences arising from the use of any information it contains.

## Dinuclear Nickel Complexes of Divergent Ni··Ni Separation Showing Ancillary Ligand Addition and Bio-macromolecular Interaction

Tufan Singha Mahapatra,<sup>a</sup> Susmitnarayan Chaudhury,<sup>a</sup> Swagata Dasgupta,<sup>a</sup> Valerio Bertolasi,<sup>b</sup> and Debashis Ray<sup>\*a</sup>

<sup>[a]</sup> Department of Chemistry, Indian Institute of Technology, Kharagpur 721 302, India  
Fax: (+91) 3222-82252; Tel: (+91) 3222-283324; E-mail: [dray@chem.iitkgp.ernet.in](mailto:dray@chem.iitkgp.ernet.in)

<sup>[b]</sup> Dipartimento di Scienze Chimiche e Farmaceutiche and Centro di Strutturistica Diffraattometrica, Università di Ferrara, via L. Borsari, 46, I44121 Ferrara, Italy.

### Abstract

Schiff base ligand HL has been utilized to build up a new family of five [Ni<sub>2</sub>] complexes, [Ni<sub>2</sub>(μ-L)(μ-OH)](ClO<sub>4</sub>)<sub>2</sub> [**1**(ClO<sub>4</sub>)<sub>2</sub>], [Ni<sub>2</sub>(μ-L)(μ-CF<sub>3</sub>CO<sub>2</sub>)<sub>2</sub>(C<sub>3</sub>H<sub>7</sub>NO)(H<sub>2</sub>O)]CF<sub>3</sub>CO<sub>2</sub>·H<sub>2</sub>O [**2a**(CF<sub>3</sub>CO<sub>2</sub>)·H<sub>2</sub>O], [Ni<sub>2</sub>(μ-L)(μ-CH<sub>3</sub>CH<sub>2</sub>CO<sub>2</sub>)<sub>2</sub>(C<sub>3</sub>H<sub>7</sub>NO)(H<sub>2</sub>O)]ClO<sub>4</sub>·C<sub>3</sub>H<sub>7</sub>NO [**2b**(ClO<sub>4</sub>)·C<sub>3</sub>H<sub>7</sub>NO], [Ni<sub>2</sub>(μ-L)(μ-CH<sub>3</sub>CO<sub>2</sub>)(μ-NCS)(NCS)(C<sub>3</sub>H<sub>7</sub>NO)] (**3a**) and [Ni<sub>2</sub>(μ-L)(μ-CH<sub>3</sub>CO<sub>2</sub>)(μ-N<sub>3</sub>)(N<sub>3</sub>)(C<sub>3</sub>H<sub>7</sub>NO)] (**3b**) in varying co-ligand environments. All the complexes have been characterized by elemental analyses, X-ray structure analysis and spectroscopic measurements. Three distinct types, dicationic, monocationic and neutral complexes, are synthesized using one pentadentate ligand HL. The Ni<sup>II</sup> centers are bridged by three sets of bridging groups resulting in a wide variation in Ni··Ni separations from 2.897 to 3.475 Å. Doubly bridged Ni<sup>II</sup> centers in edge-shared square planar environment provide shortest Ni··Ni separation in **1**<sup>2+</sup>. Whereas combination of other bridges from carboxylate, azide and isothiocyanate ancillary ligands result cationic and neutral [Ni<sub>2</sub>] complexes **2**<sup>+</sup> and **3** having longer intermetallic separations. Modulation of Ni··Ni separation in synthetic complexes is fascinating in relation to the involvement and stabilization of the dinickel motif in the catalytic transition state of urease. Interaction and binding of cationic complexes (**1-2b**) with human serum albumin (HSA) and calf thymus-DNA have been examined using spectroscopic techniques. Tryptophan fluorescence quenching of HSA by cationic bimetallic complexes (**1**, **2a** and **2b**) featuring hydrophobic ligand environment show

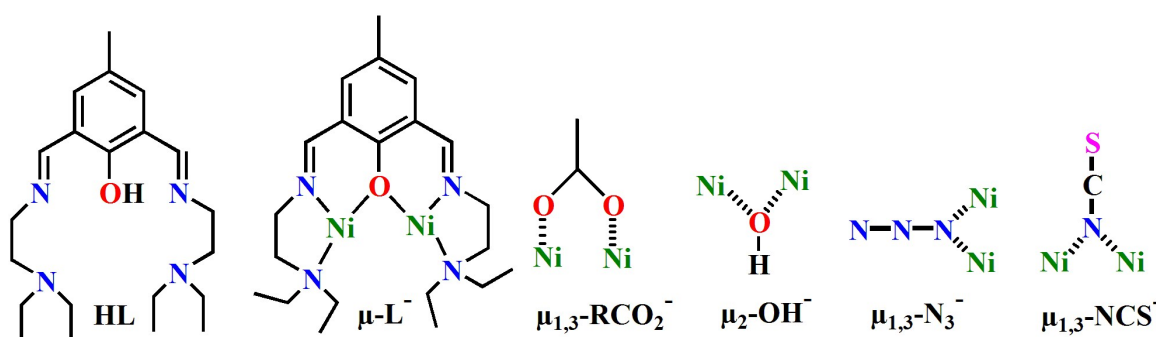
spontaneous and favorable interactions in the order **2a** > **2b** > **1**. For the interaction study with CT-DNA, nearly planar complex **1** binds more efficiently than **2a** and **2b** in octahedral coordination geometry.

## Introduction

Urease (urea amidohydrolases, EC 3.5.1.5) are nickel metalloenzymes extensively present in several bacteria, plants, fungi, algae, and some invertebrates, as well as in soils.<sup>1</sup> Its active site contains an asymmetric binuclear nickel active site where two hydroxido-bridged nickel ions are separated by a distance of  $\sim 3.5$  Å that catalyzes the hydrolysis of urea to carbamate and ammonium ions.<sup>2</sup> These two ions are further bridged by a carbamylated lysine through its O atoms. Thus biomimetic structural and functions studies using  $\text{HO}^-$  and  $\text{RCO}_2^-$  bridged  $[\text{Ni}_2]$  complexes remain a significant tool for understanding the importance of  $\text{Ni}\cdots\text{Ni}$  separations in the enzymatic activity.<sup>3</sup> Studies on binuclear  $[\text{Ni}_2]$  complexes are relevant in this regard because during hydrolysis the urea molecule binds to the more electrophilic nickel(II) ion with the O atom of its carbonyl group, which in turn makes the carbonyl C atom more electrophilic. The situation thus leads to the hydrolysis of urea by nucleophilic attack of bridging hydroxide ion on the carbonyl C atom of the substrate.<sup>4</sup> Another promising area for exploring the biological activity of the nickel(II) complexes is protein-complex binding study. Protein interactions play an important role in many biochemical processes in both the healthy and diseased state, and information about the interactions of metal ions bound to various organic ligands with serum albumin can help to reveal the role of albumins in above mentioned states.<sup>5</sup> Human serum albumin (HSA) is the most abundant protein in human blood plasma and can bind and transport a range of molecules with reversibility and high affinity.<sup>6</sup> HSA consists of a single polypeptide chain of 585 amino acids with less number of Trp and Met residues, and an abundance of Cys and charged residues.<sup>7</sup> Identification of amino terminal copper(II) and nickel(II) binding motif in HSA also point to the fact that nickel(II) complexes, both mononuclear and dinuclear, can show promises for albumin binding capacity.<sup>8</sup> In comparison to mononuclear complex entity the protein interactions with binuclear systems is important for their influence or inhibition through selective recognition. DNA binding and cleavage property is also an encouraging area for

exploring the biological activity of such nickel(II) complexes when they recognize nucleic acids.<sup>9</sup> Those metal complexes would be interesting which damage DNA and block DNA synthesis indirectly through inhibition of nucleic acid precursor biosynthesis.<sup>10</sup> Many such metal complexes are known to interact with DNA mainly through the three non-covalent approaches: intercalation, groove binding and electronic control.<sup>10a</sup> In this context, several studies have been made for DNA binding using mononuclear nickel(II) complexes<sup>9a-9e</sup> but relatively few studies have been reported on dinuclear nickel(II) complexes.<sup>9f-9h</sup>

We have been interested in the coordination behavior and dinucleating properties of the ligand HL (Scheme 1, 2,6-*bis*-[(2-diethylamino-ethylimino)-methyl]-4-methyl-phenol) towards two Ni<sup>2+</sup> ions in presence of various anions like CF<sub>3</sub>CO<sub>2</sub><sup>-</sup>, CH<sub>3</sub>CH<sub>2</sub>CO<sub>2</sub><sup>-</sup>, MeCO<sub>2</sub><sup>-</sup>, HO<sup>-</sup>, SCN<sup>-</sup>, N<sub>3</sub><sup>-</sup> and coordinated solvents like H<sub>2</sub>O and DMF (dimethylformamide). In a small piece of work the coordination behavior of HL has earlier been established for Cu<sup>2+</sup> ions.<sup>11</sup> The utilization of [L]<sup>-</sup> and RCO<sub>2</sub><sup>-</sup>, HO<sup>-</sup>, N<sub>3</sub><sup>-</sup> and NCS<sup>-</sup> lead to different types of intermetallic bridges between the two Ni atoms (Scheme 1). Reported here are the stable dinuclear Ni(II) complexes of HL in varying coordination geometry with three different intermetallic bridging sites. Herein, we report the synthesis, crystal structure, spectral characterization, and human serum albumin (HSA) protein and CT-DNA binding affinity of the synthesized [Ni<sub>2</sub>] complexes.



**Scheme 1.** Ligand HL and observed binding modes of [L]<sup>-</sup>, RCO<sub>2</sub><sup>-</sup>, HO<sup>-</sup>, N<sub>3</sub><sup>-</sup>, SCN<sup>-</sup>

## Experimental section

### Materials used for synthesis

The chemicals used for the work were obtained from the following sources: nickel(II) carbonate from Universal Laboratory (India), trifluoroacetic acid, propanoic acid, sodium azide and triethylamine from E. Merck (India), ammonium thiocyanate from S.D. Fine Chemicals (India), nickel(II) acetate from CDH (P) Ltd (India) and N,N-diethyl-1,2-diaminoethane from Alfa Aesar. 2,6-Diformyl-4-methylphenol (2-hydroxy-5-methylbenzene-1,3-dicarbaldehyde) was prepared following a literature procedure.<sup>12</sup> Ni(ClO<sub>4</sub>)<sub>2</sub>·6H<sub>2</sub>O was prepared by treating nickel(II) carbonate to a solution of perchloric acid (20 mL, 70%) in 20 mL of water under constant glass-rod stirring until effervescence had stopped and crystallized the filtered solution after concentration on a water bath at room temperature. CF<sub>3</sub>CO<sub>2</sub>Na and CH<sub>3</sub>CH<sub>2</sub>CO<sub>2</sub>Na were prepared by treating trifluoroacetic acid (17 g, 0.15 mol) and propionic acid (11 g, 0.15 mol) with solid sodium hydroxide (6.0 g, 0.15 mol) followed by concentration and crystallization on a water bath. Ni(CF<sub>3</sub>CO<sub>2</sub>)<sub>2</sub>·4H<sub>2</sub>O was synthesized by adding nickel(II) carbonate to a solution of trifluoroacetic acid (20 mL, 99%) in 20 mL of water under constant glass-rod stirring until effervescence had stopped. Then the solution was filtered, and the clear filtrate was kept over a water bath until a solid started to precipitate. The solution was then filtered through suction and dried in vacuum. Human serum albumin (fatty acid free, fraction V) was obtained from Sigma-Aldrich (USA). Calf thymus DNA (CT-DNA) and ethidium bromide (EB) were purchased from SRL (India). Solutions of complexes **1**(ClO<sub>4</sub>)<sub>2</sub>, **2a**(CF<sub>3</sub>CO<sub>2</sub>)·H<sub>2</sub>O and **2b**(ClO<sub>4</sub>)·C<sub>3</sub>H<sub>7</sub>NO were prepared in absolute ethanol and subsequent dilutions were made with 10 mM phosphate buffer (pH 7.4) with reduction in concentration below 5%. All other chemicals and solvents were reagent grade materials and were used as received without further purification.

**Caution!!** *Although no such behavior was observed during the present work, azide and perchlorate salts involving organic ligands are potentially explosive; such compounds should be synthesized and used in small quantities, and treated with utmost care at all times.*

### Syntheses

**HL.** To a MeOH solution (30 mL) of 2,6-diformyl-4-methylphenol (0.820 g, 5 mmol), N,N-diethyl-1,2-diaminoethane (1.40 mL, 1.16 g, 10 mmol) in 1:2 ratio was added drop

wise at room temperature. Two hour stirring followed by evaporation of solvent under vacuum give an orange colored semi-solid product. The semi-solid substance was characterized by NMR spectroscopy and used directly for reactions with nickel(II) salts without further purification. Yield: 1.75 g (97%).  $^1\text{H}$  NMR (400 MHz,  $\text{CDCl}_3$ , ppm):  $\delta$  8.50 (2H, br s, imine H), 7.39 (2H, s, ArH), 3.68-3.64 (4H, t,  $-\text{C}=\text{N}-\underline{\text{CH}_2}$ ), 2.75-2.71 (4H, t,  $-\text{NEt}_2-\underline{\text{CH}_2}$ ), 2.58-2.53 (8H, q,  $-\text{N}-\underline{\text{CH}_2}$ ), 2.24 (3H, s, Ar- $\text{CH}_3$ ), 1.00-0.983 (12H, t,  $\text{CH}_3$ ).

**$[\text{Ni}_2(\mu\text{-L})(\mu\text{-OH})(\text{ClO}_4)_2][\text{ClO}_4]_2$** . To a MeOH solution (10 mL) of HL (0.360 g, 1.00 mmol), another MeOH solution (10 mL) of  $\text{Ni}(\text{ClO}_4)_2 \cdot 6\text{H}_2\text{O}$  (0.730 g, 2.0 mmol) was added slowly with stirring at ambient temperature in air. After 10 min  $\text{NEt}_3$  (0.139 mL, 0.1 g, 1.00 mmol) in methanol was added and the resulting brown solution was further stirred for 3 h. Then the mixture was filtered and the filtrate was allowed to stand for slow evaporation for 7 days to get deep brown needle shaped crystals suitable for X-ray analysis. Yield: 0.540 g, 78%. Anal. Calcd. for  $\text{C}_{21}\text{H}_{36}\text{Ni}_2\text{N}_4\text{O}_{10}\text{Cl}_2$  (692.82 g  $\text{mol}^{-1}$ ): C, 36.41; H, 5.24; N, 8.09. Found: C, 36.76; H, 5.50; N, 7.91. Selected FT-IR bands: (KBr,  $\text{cm}^{-1}$ ; s = strong, vs = very strong, m = medium, br = broad) 3447(br), 1636(s), 1560(m), 1458(m), 1384(m), 1325(m), 1093(vs), 624(m). Molar conductance,  $\Lambda_{\text{M}}$ : (MeCN solution) 290  $\Omega^{-1} \text{cm}^2 \text{mol}^{-1}$ . UV-vis spectra [ $\lambda_{\text{max}}$ , nm ( $\epsilon$ ,  $\text{L mol}^{-1} \text{cm}^{-1}$ ): (MeOH solution) 395 (5800), 254 (19900); (solid, reflectance) 491, 388, 241. HRMS ( $m/z$ ,  $\text{ESI}^+$ ): found for  $[\{\text{Ni}_2(\text{L})(\text{OH})\}\text{H}]^+ = 493.1425$  (calcd 493.1623).

**$[\text{Ni}_2(\mu\text{-L})(\mu\text{-CF}_3\text{CO}_2)_2(\text{C}_3\text{H}_7\text{NO})(\text{H}_2\text{O})](\text{CF}_3\text{CO}_2) \cdot \text{H}_2\text{O}$  [**2a**( $\text{CF}_3\text{CO}_2$ ) $\cdot\text{H}_2\text{O}$ ]** and  **$[\text{Ni}_2(\mu\text{-L})(\mu\text{-CH}_3\text{CH}_2\text{CO}_2)_2(\text{C}_3\text{H}_7\text{NO})(\text{H}_2\text{O})]\text{ClO}_4 \cdot \text{C}_3\text{H}_7\text{NO}$  [**2b**( $\text{ClO}_4$ ) $\cdot\text{C}_3\text{H}_7\text{NO}$ ]**. **Method A from direct reaction.** HL (0.360 g, 1.00 mmol) was dissolved in DMF (15 mL) and to this a MeOH solution (5 mL) of nickel(II) trifluoroacetate (0.712 g, 2 mmol) was added slowly under stirring condition and the resulting brown solution was further stirred for ca. 2 h. For complex **2b**, a mixture of  $\text{Ni}(\text{ClO}_4)_2 \cdot 6\text{H}_2\text{O}$  (0.730 g, 2.0 mmol) and sodium propionate (0.192 g, 2 mmol) were used instead of nickel(II) trifluoroacetate as used in case of **2a**. The filtered solutions on standing at room temperature produced diffraction quality light green prismatic and block shaped single crystals of **2a**( $\text{CF}_3\text{CO}_2$ ) $\cdot\text{H}_2\text{O}$  and **2b**( $\text{ClO}_4$ ) $\cdot\text{C}_3\text{H}_7\text{NO}$  after 18 and 21 days, respectively. Yield: 0.666 g, 72% (**2a**) and 0.630 g, 71% (**2b**).

**Method B from 1.** Addition of an aqueous solution of sodium trifluoroacetate (0.272 g, 2 mmol) or sodium propionate (0.192 g, 2 mmol) to  $1(\text{ClO}_4)_2$  (0.692 g, 1 mmol) in 15 mL of DMF with stirring at room temperature provided  $2\mathbf{a}(\text{CF}_3\text{CO}_2)\cdot\text{H}_2\text{O}$  or  $2\mathbf{b}(\text{ClO}_4)\cdot\text{C}_3\text{H}_7\text{NO}$ , respectively. The reaction mixtures were stirred for 2 h and the resulting brown solutions were filtered and kept at room temperature for evaporation. The color of the solutions change to light green in due course of slow evaporation and light green crystalline compound containing diffraction quality single crystals were obtained over a period of 3 weeks on standing at room temperature. Yield: 0.703 g, 76% ( $2\mathbf{a}$ ) and 0.612 g, 69% ( $2\mathbf{b}$ ).

Complex [ $2\mathbf{a}(\text{CF}_3\text{CO}_2)\cdot\text{H}_2\text{O}$ ]. Anal. Calcd. for  $\text{C}_{30}\text{H}_{46}\text{Ni}_2\text{N}_5\text{O}_{10}\text{F}_9$  ( $925.10 \text{ g mol}^{-1}$ ): C, 38.95; H, 5.01; N, 7.57. Found: C, 38.72; H, 4.93; N, 7.34. Selected FT-IR bands: (KBr,  $\text{cm}^{-1}$ ; s = strong, vs = very strong, m = medium, br = broad) 3420(br), 1707(vs), 1676(vs), 1548(m), 1450(m), 1206(vs), 1147(s), 725(m). Molar conductance,  $\Lambda_M$ : (MeCN solution)  $135 \Omega^{-1} \text{ cm}^2 \text{ mol}^{-1}$ . UV-vis spectra [ $\lambda_{\text{max}}$ , nm ( $\epsilon$ ,  $\text{L mol}^{-1} \text{ cm}^{-1}$ ): (MeOH solution) 391 (6500), 255 (22500); (solid, reflectance) 614, 379, 251. HRMS ( $m/z$ ,  $\text{ESI}^+$ ): found for  $[\text{Ni}_2(\text{L})(\text{CF}_3\text{CO}_2)_2]^+ = 701.1223$  (calcd 701.1219).

Complex [ $2\mathbf{b}(\text{ClO}_4)\cdot\text{C}_3\text{H}_7\text{NO}$ ]. Anal. Calcd. for  $\text{C}_{33}\text{H}_{61}\text{Ni}_2\text{N}_6\text{O}_{12}\text{Cl}$  ( $886.70 \text{ g mol}^{-1}$ ): C, 44.70; H, 6.93; N, 9.48. Found: C, 44.83; H, 7.10; N, 9.49. Selected FT-IR bands: (KBr,  $\text{cm}^{-1}$ ; s = strong, vs = very strong, m = medium, br = broad) 3422(br), 1660(s), 1607(vs), 1550(m), 1426(m), 1089(vs), 1007(m), 624(m). Molar conductance,  $\Lambda_M$ : (MeCN solution)  $125 \Omega^{-1} \text{ cm}^2 \text{ mol}^{-1}$ . UV-vis spectra [ $\lambda_{\text{max}}$ , nm ( $\epsilon$ ,  $\text{L mol}^{-1} \text{ cm}^{-1}$ ): (MeOH solution) 391 (5700), 254 (18400); (solid, reflectance) 623, 368, 250. HRMS ( $m/z$ ,  $\text{ESI}^+$ ): found for  $[\text{Ni}_2(\text{L})(\text{CH}_3\text{CH}_2\text{CO}_2)]^+ = 621.2078$  (calcd 621.2335).

**$[\text{Ni}_2(\mu\text{-L})(\mu\text{-CH}_3\text{CO}_2)(\mu\text{-NCS})(\text{NCS})(\text{C}_3\text{H}_7\text{NO})]$  ( $3\mathbf{a}$ ) and  $[\text{Ni}_2(\mu\text{-L})(\mu\text{-CH}_3\text{CO}_2)(\mu\text{-N}_3)(\text{N}_3)(\text{C}_3\text{H}_7\text{NO})]$  ( $3\mathbf{b}$ ). Direct Methods.** HL (0.360 g, 1.00 mmol) was dissolved in 15 mL of DMF and a MeOH solution (4 mL) of  $\text{Ni}(\text{CH}_3\text{CO}_2)_2\cdot 4\text{H}_2\text{O}$  (0.500 g, 2 mmol) was added slowly under stirring condition for 30 min to get a light green solution. Next aqueous solution of  $\text{NH}_4\text{SCN}$  (0.152 g, 2 mmol for complex  $3\mathbf{a}$ ) or  $\text{NaN}_3$  (0.130 g, 2 mmol for complex  $3\mathbf{b}$ ) was added to the reaction mixture and stirred for another 2 h. Evaporation of the respective filtrates provide light green block shaped single crystals of  $3\mathbf{a}$  and  $3\mathbf{b}$  after 14 and 10 days, respectively.

**3a.** Yield: 0.587 g, 81%. Anal. Calcd. for  $C_{28}H_{45}Ni_2N_7O_4S_2$  ( $725.23 \text{ g mol}^{-1}$ ): C, 46.37; H, 6.25; N, 13.52. Found: C, 46.02; H, 6.56; N, 13.16. Selected FT-IR bands: (KBr,  $\text{cm}^{-1}$ ; s = strong, vs = very strong, m = medium, br = broad) 2100(s), 2015(vs), 1653(vs), 1583(s), 1457(m), 1423(m), 1382(m), 1339(m), 737(m). Molar conductance,  $\Lambda_M$ : (MeCN solution)  $15 \Omega^{-1} \text{ cm}^2 \text{ mol}^{-1}$ . UV-vis spectra [ $\lambda_{\text{max}}$ , nm ( $\epsilon$ ,  $\text{L mol}^{-1} \text{ cm}^{-1}$ )]: (MeOH solution) 393 (6000), 256 (21500); (solid, reflectance) 617, 364, 248. HRMS ( $m/z$ ,  $\text{ESI}^+$ ): found for  $[\{\text{Ni}_2(\text{L})(\text{NCS})(\text{NCS})\}\text{H}]^+ = 592.1382$  (calcd 592.1099).

**3b.** Yield: 0.590 g, 85%. Anal. Calcd. for  $C_{26}H_{45}Ni_2N_{11}O_4$  ( $693.11 \text{ g mol}^{-1}$ ): C, 45.06; H, 6.54; N, 22.23. Found: C, 44.91; H, 6.56; N, 22.02. Selected FT-IR bands: (KBr,  $\text{cm}^{-1}$ ; s = strong, vs = very strong, m = medium, br = broad) 2072(s), 2042(s), 1651(s), 1583(s), 1454(m), 1417(m), 1336(m). Molar conductance,  $\Lambda_M$ : (MeCN solution)  $23 \Omega^{-1} \text{ cm}^2 \text{ mol}^{-1}$ . UV-vis spectra [ $\lambda_{\text{max}}$ , nm ( $\epsilon$ ,  $\text{L mol}^{-1} \text{ cm}^{-1}$ )]: (MeOH solution) 397 (8600), 253 (27500); (solid, reflectance) 618, 388, 251. HRMS ( $m/z$ ,  $\text{ESI}^+$ ): found for  $[\{\text{Ni}_2(\text{L})(\text{N}_3)(\text{N}_3)\}\text{H}]^+ = 562.1594$  (calcd 562.1735).

### Physical measurements

Elemental analyses (C, H and N) were performed with a Perkin-Elmer model 240C elemental analyzer. FT-IR spectra ( $4000\text{--}400 \text{ cm}^{-1}$ ) were recorded on KBr disks with a Perkin-Elmer 883 spectrometer. The solution electrical conductivity data was obtained using a Unitech type U131C digital conductivity meter with solute concentration of about  $10^{-3} \text{ M}$ . UV-vis spectra were recorded in Shimadzu UV 3100 UV-vis-NIR spectrophotometer using a 1 cm quartz cuvette. The diffuse reflectance spectra (DRS) were measured with a Cary model 5000 UV-vis-NIR spectrophotometer. The fluorescence spectra were recorded in Fluoromax-4 (Horiba Jobin Yvon) spectrofluorometer and 1 cm quartz cell. Slit width and integration time were fixed at 5 nm and 0.3 s respectively. High-resolution mass spectra (ESI) were recorded using the Xevo G2 TOF mass spectrometer. Powder X-ray diffraction (PXRD) patterns were measured on a BRUKER AXS X-ray diffractometer (40 kV, 20 mA) using  $\text{Cu-K}\alpha$  radiation ( $\lambda = 1.5418 \text{ \AA}$ ) within  $5\text{--}50^\circ$  ( $2\theta$ ) range and a fixed-time counting of 4 s at  $25^\circ\text{C}$ . TGA of the complexes were carried out using a Netzsch STA 409 PC Luxx with a heating rate of  $10^\circ\text{C min}^{-1}$  under  $\text{O}_2$  atmosphere in a temperature range of  $25\text{--}800^\circ\text{C}$ .  $^1\text{H}$  NMR (400 MHz) spectrum was recorded on a Bruker ACF200 spectrometer.

### Hirshfeld surface analysis

Hirshfeld surfaces were mapped using Crystal Explorer (version 3.1) software using the crystal structure coordinates of CIF files.<sup>13</sup> Graphical plots of the molecular Hirshfeld surfaces are mapped with normalized contact distance ( $d_{\text{norm}}$ ) using a color code of red–white–blue, where red spots indicate shorter contacts, white regions highlight contacts around the van der Waals distance, and the blue areas are for longer contacts. Two more colored properties, shape index and curvedness, have also been specified based on the shape and the local curvature of the surfaces.

### HSA binding study

The study was carried out by monitoring tryptophan fluorescence quenching experiments using human serum albumin (HSA, 2  $\mu\text{M}$ ) in 10 mM phosphate buffer (pH 7.4). The fluorescence emission spectra of Trp residue of HSA was recorded at room temperature by setting the excitation wavelength at 295 nm and scan range of 305–445 nm. Fluorometric titration experiments were carried out by using 3 mL solutions of 2  $\mu\text{M}$  HSA with successive addition of **1**(ClO<sub>4</sub>)<sub>2</sub>, **2a**(CF<sub>3</sub>CO<sub>2</sub>)·H<sub>2</sub>O and **2b**(ClO<sub>4</sub>)·C<sub>3</sub>H<sub>7</sub>NO from concentration range 0 to 23  $\mu\text{M}$ . Each spectrum was corrected with respect to the corresponding blank.

### DNA binding experiment

The DNA binding ability of cationic **1**(ClO<sub>4</sub>)<sub>2</sub>, **2a**(CF<sub>3</sub>CO<sub>2</sub>)·H<sub>2</sub>O and **2b**(ClO<sub>4</sub>)·C<sub>3</sub>H<sub>7</sub>NO were studied using UV–vis and fluorescence spectroscopy. The UV–vis titrations of each complexes were carried out with the addition of increasing amount of CT-DNA (0–50  $\mu\text{M}$ ) in 10 mM phosphate buffer (pH 7.4) to a fixed concentration of metal complex (100  $\mu\text{M}$ ). The scan range was set at 700–200 nm. The concentration of CT-DNA was determined from the absorbance values at 260 nm<sup>14</sup> using molar extinction coefficient ( $\epsilon = 6600 \text{ M}^{-1} \text{ cm}^{-1}$ ).

The relative DNA binding ability of the complexes were also studied with fluorescence spectroscopy using an EB-bound CT-DNA solution in 10 mM phosphate buffer (pH 7.4) medium. The fluorescence spectra were recorded at room temperature with excitation at 480 nm and emission at 597 nm. The fluorescence emission spectra of CT-DNA-EB system were collected following successive addition of the nickel(II) complexes (0–25.6

$\mu\text{M}$ ), while CT-DNA and EB concentration were maintained at 50  $\mu\text{M}$  and 5  $\mu\text{M}$ , respectively.

### X-ray crystallography

X-ray diffraction data on appropriate single crystals of **1**(ClO<sub>4</sub>)<sub>2</sub>, **2b**(ClO<sub>4</sub>)·C<sub>3</sub>H<sub>7</sub>NO, **3a** and **3b** were collected on a Bruker SMART APEX-II CCD diffractometer, equipped with a graphite monochromator and Mo-K<sub>α</sub> radiation ( $\lambda = 0.71073 \text{ \AA}$ ) at 293 K with a counting time of 5 s per frame. Space group determination, data integration and reduction were performed with XPREP and SAINT software.<sup>15</sup> The Structures were solved using the direct method through the SHELXS-97<sup>16</sup> and refined with full-matrix least squares on F<sup>2</sup> using the SHELXL-97<sup>17</sup> program package incorporated into WINGX system Version 1.80.05.<sup>18</sup> Multiscan empirical absorption corrections were applied to the data using the program SADABS.<sup>19</sup> The data for **2a**(CF<sub>3</sub>CO<sub>2</sub>)·H<sub>2</sub>O was collected at room temperature using a Nonius Kappa CCD diffractometer. The data set was integrated with the Denzo-SMN package<sup>20</sup> and corrected for Lorentz, polarization, and absorption effects (SORTAV).<sup>21</sup> The structure was solved by direct methods (SIR97)<sup>22</sup> and the calculations were performed using SHELXL-97<sup>17</sup> and PARST<sup>23</sup> implemented in WINGX suite of programs.<sup>24</sup> All non-hydrogen atoms were refined anisotropically. The H atoms were introduced in calculated positions and refined with fixed geometry and riding thermal parameters with respect to their carrier atoms. The locations of the heaviest atoms (Ni) were determined easily, and the O, N, and C atoms were subsequently determined from the difference Fourier maps. Crystallographic diagrams were presented using DIAMOND software.<sup>25</sup> Information concerning X-ray data collection and crystal structure refinement is summarized in Table 1. Crystallographic data (excluding structure factors) have been deposited with the Cambridge Crystallographic Data Centre as supplementary publications CCDC-1402077, 1402078, 1402079, 1402080, 1402081.

**Table 1.** Crystallographic data

Compound reference	<b>1</b> (ClO <sub>4</sub> ) <sub>2</sub>	<b>2a</b> (CF <sub>3</sub> CO <sub>2</sub> )·H <sub>2</sub> O	<b>2b</b> (ClO <sub>4</sub> )·C <sub>3</sub> H <sub>7</sub> NO	<b>3a</b>	<b>3b</b>
Chemical formula	C <sub>21</sub> H <sub>36</sub> N <sub>4</sub> Ni <sub>2</sub> O <sub>2</sub> ·2(ClO <sub>4</sub> )	C <sub>28</sub> H <sub>44</sub> F <sub>6</sub> N <sub>5</sub> Ni <sub>2</sub> O <sub>7</sub> ·C <sub>2</sub> F <sub>3</sub> O <sub>2</sub> ·H <sub>2</sub> O	C <sub>30</sub> H <sub>54</sub> N <sub>5</sub> Ni <sub>2</sub> O <sub>7</sub> ·ClO <sub>4</sub> ·C <sub>3</sub> H <sub>7</sub> NO	C <sub>28</sub> H <sub>45</sub> N <sub>7</sub> Ni <sub>2</sub> O <sub>4</sub> S <sub>2</sub>	C <sub>26</sub> H <sub>45</sub> N <sub>11</sub> Ni <sub>2</sub> O <sub>4</sub>
Formula Mass	692.82	925.10	886.75	725.23	693.11
Crystal system	Monoclinic	Triclinic	Monoclinic	Orthorhombic	Monoclinic

Space group	$P2_1/n$	$P\bar{1}$	$P2_1/n$	$Fdd2$	$P2_1/c$
Crystal color	Brown	Light green	Light green	Light green	Light green
Crystal size/mm <sup>3</sup>	0.32x0.25x0.20	0.48x0.36x0.26	0.36x0.28x0.22	0.40x0.32x0.26	0.34x0.29x0.21
$a/\text{\AA}$	7.5074(6)	11.6655(1)	19.664(3)	17.461(3)	10.3693(9)
$b/\text{\AA}$	15.9840(13)	16.9475(1)	11.6297(18)	67.604(9)	35.460(3)
$c/\text{\AA}$	23.982(2)	22.7678(2)	20.591(3)	12.0678(17)	18.8761(15)
$\alpha/^\circ$	90.00	74.2190(4)	90.00	90.00	90.00
$\beta/^\circ$	96.482(3)	87.0926(4)	117.270(4)	90.00	104.288(2)
$\gamma/^\circ$	90.00	75.7040(4)	90.00	90.00	90.00
$V/\text{\AA}^3$	2859.4(4)	4196.77(6)	4185.5(11)	14246(3)	6726.0(10)
$Z$	4	4	4	16	8
$D_c/\text{g cm}^{-3}$	1.609	1.464	1.407	1.353	1.369
$\mu$ (mm <sup>-1</sup> )	1.562	0.991	1.027	1.215	1.167
F(000)	1440	1912	1872	6112	2928
$T/^\circ\text{K}$	295	295	295	295	295
Total reflns	32360	54669	51533	36794	69063
R(int)	0.099	0.0389	0.0421	0.1302	0.0435
Unique reflns	4886	19828	8467	6317	13925
Observed reflns ( $I > 2\sigma(I)$ )	3285	14370	6939	3474	8672
Parameters	359	1051	497	392	776
$R_1$ ( $I > 2\sigma(I)$ )	0.0863	0.0618	0.0377	0.0874	0.0578
$wR_2$ (all reflns)	0.2280	0.1964	0.1046	0.1526	0.1679
GOF ( $F^2$ )	1.116	1.058	1.058	1.130	1.043
Largest diff peak and hole (e $\text{\AA}^{-3}$ )	1.352, -0.515	1.143, -0.630	0.929, -0.556	0.352, -0.322	0.886, -0.745
CCDC number	1402077	1402078	1402079	1402080	1402081

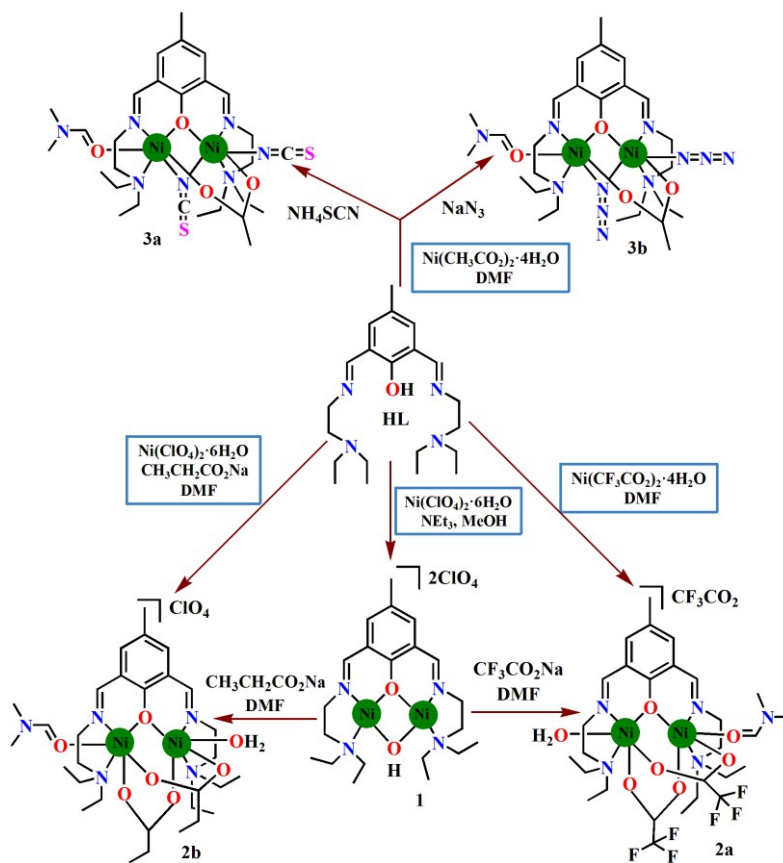
$$R_1 = \Sigma(|F_o| - |F_c|) / \Sigma|F_o|, wR_2 = [\Sigma w(|F_o| - |F_c|)^2 / \Sigma w(F_o)^2]^{1/2}, w = 0.75 / (\sigma^2(F_o) + 0.0010F_o^2).$$

## Results and discussion

**Synthetic protocol.** The ligand 2,6-bis-[(2-diethylamino-ethylimino)-methyl]-4-methylphenol (HL) was obtained from room temperature Schiff base reaction of 2,6-diformyl-4-methylphenol and N,N-diethyl-1,2-diaminoethane in 1:2 molar ratio (Scheme S1). The coordination behavior of HL with nickel(II) ions have been examined systematically in presence of various added ancillary ligands as summarized in Scheme 2. The reaction of  $\text{Ni}(\text{ClO}_4)_2 \cdot 6\text{H}_2\text{O}$  with HL and  $\text{NEt}_3$  in MeOH afforded a brownish solution, from which  $\mathbf{1}(\text{ClO}_4)_2$  was separated as brown solid in 78% yield (eq 1).

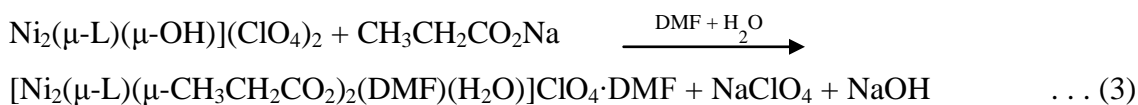
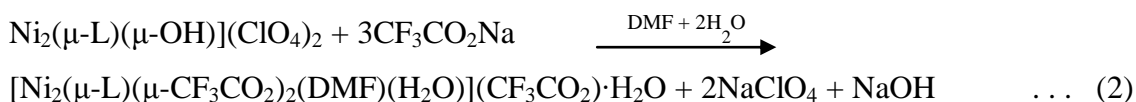


The elemental analysis, molar conductivity, mass spectral and single crystal X-ray diffraction data clearly establish  $1(\text{ClO}_4)_2$  as  $[\text{Ni}_2(\mu\text{-L})(\mu\text{-OH})](\text{ClO}_4)_2$  as against any other possibilities.

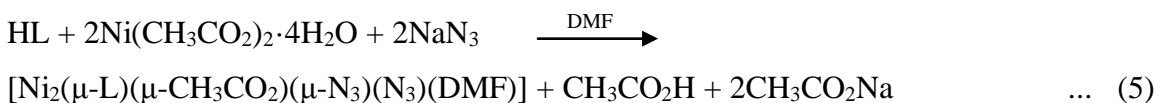


**Scheme 2.** Summary of the synthetic routes and transformations

Complex  $1(\text{ClO}_4)_2$  showed ancillary ligand addition reactions with two sodium salts of carboxylic acids to provide two triple bridged  $\mu$ -phenoxo-bis( $\mu$ -carboxylate) dinickel(II) complexes **2a**( $\text{CF}_3\text{CO}_2$ ) $\cdot\text{H}_2\text{O}$  and **2b**( $\text{ClO}_4$ ) $\cdot\text{C}_3\text{H}_7\text{NO}$  in good yield (Scheme 2; eqs. 2 and 3).



Direct reactions of HL with  $\text{Ni}(\text{CF}_3\text{CO}_2)_2 \cdot 4\text{H}_2\text{O}$  and 1:1 mixture of  $\text{Ni}(\text{ClO}_4)_2 \cdot 6\text{H}_2\text{O}$  and  $\text{CH}_3\text{CH}_2\text{CO}_2\text{Na}$  in DMF resulted **2a**( $\text{CF}_3\text{CO}_2$ ) $\cdot\text{H}_2\text{O}$  and **2b**( $\text{ClO}_4$ ) $\cdot\text{C}_3\text{H}_7\text{NO}$  respectively. Reactions with  $\text{Ni}(\text{CH}_3\text{CO}_2)_2 \cdot 4\text{H}_2\text{O}$  only have not resulted corresponding acetato-bridged analogues. But the use of  $\text{NH}_4\text{SCN}$  or  $\text{NaN}_3$  in the reactions afforded new type of isothiocyanato- and azido-bridged dinuclear complexes **3a** and **3b** (Scheme 2; eqs. 4 and 5).



The elemental analysis, molar conductivity and high resolution mass spectral (HRMS) data initially indicate the formulation of the complexes which finally confirmed by single crystal X-ray structure determination. The molar conductivity values at 298 K for **1**( $\text{ClO}_4$ ) $_2$ –**3b** are 290, 135, 125, 15 and 23  $\Omega^{-1} \text{cm}^2 \text{M}^{-1}$ , respectively. Examination of the values reveals that complex **1**( $\text{ClO}_4$ ) $_2$  is a 2:1 electrolyte,<sup>26</sup> whereas the values for complexes **2a**( $\text{CF}_3\text{CO}_2$ ) $\cdot\text{H}_2\text{O}$  and **2b**( $\text{ClO}_4$ ) $\cdot\text{C}_3\text{H}_7\text{NO}$  correspond to 1:1 electrolyte type in solution, which nicely corroborates with their solid-state structures (*vide supra*). The solution stability of **3a** and **3b** lead to the values for non-electrolyte nature.

**Presence of coordinating and ancillary ligands.** The sharp peaks at 1635, 1676, 1660, 1653 and 1651  $\text{cm}^{-1}$  respectively for **1**, **2a**, **2b**, **3a** and **3b** are assigned for the characteristic  $\bar{\nu}_{\text{C=N}}$  stretching frequencies of  $\text{Ni}^{\text{II}}$ –bound  $\text{L}^-$  (Fig. S1). The presence of nickel-bound bridging  $\text{HO}^-$  groups in **1** is detected by the presence of broad and medium intensity at 3396  $\text{cm}^{-1}$ . The presence of coordinated and lattice water molecules in **2a** and coordinated molecule water in **2b** show broad and medium intensity bands at 3420 and 3422  $\text{cm}^{-1}$ , respectively. In **1** and **2b** the triply degenerate asymmetric ( $\nu_3$ ) stretching vibration for uncoordinated perchlorate anions are observed at 1093 and 1089  $\text{cm}^{-1}$ , respectively. Whereas the asymmetric Cl–O bending vibrations for these complexes appear at 624  $\text{cm}^{-1}$ .<sup>27</sup> The  $\mu_{1,3}$ -bridging by carboxylates are nicely demonstrated by their characteristic stretching frequencies. Asymmetric ( $\bar{\nu}_{\text{as}(\text{COO})}$ ) and symmetric ( $\bar{\nu}_{\text{s}(\text{COO})}$ ) carboxylates stretching vibrations for **2a** and **2b**, bearing double carboxylato bridges, at

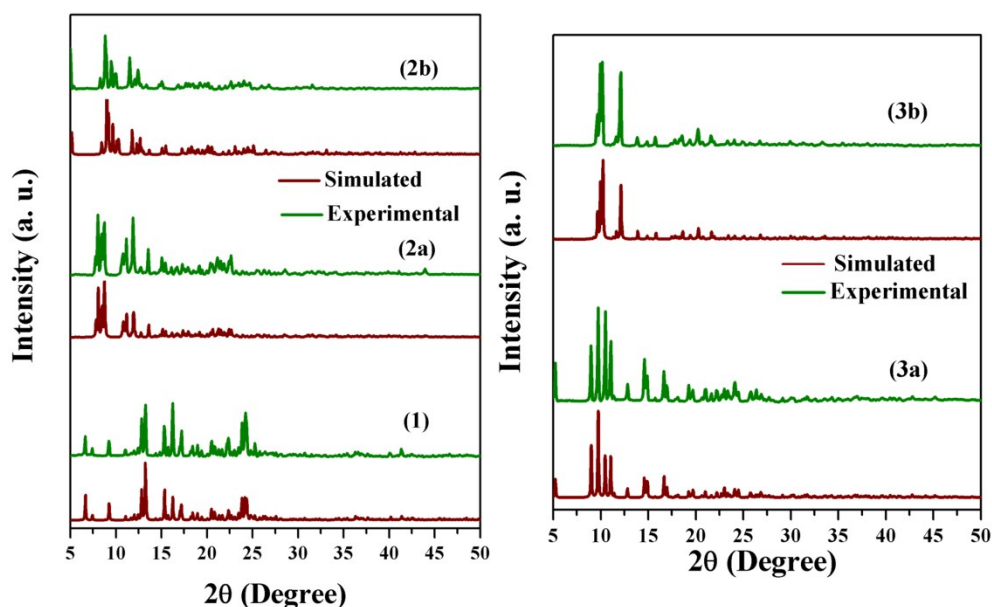
1707, 1450  $\text{cm}^{-1}$  ( $\Delta \bar{\nu} = 257 \text{ cm}^{-1}$ ) and 1607, 1425  $\text{cm}^{-1}$  ( $\Delta \bar{\nu} = 182 \text{ cm}^{-1}$ ), respectively support the proposition for this binding mode.<sup>28</sup> In case of trifluoroacetato bridging in **2a**, the asymmetric stretching vibration band is shifted to higher frequency region with higher  $\Delta \bar{\nu}$  value [ $\Delta \bar{\nu} = \bar{\nu}_{\text{as(COO)-}} - \bar{\nu}_{\text{s(COO)}}$ ] may be due to the presence of three strongly electron withdrawing fluorine atoms.<sup>29</sup> The values for **3a** and **3b**, bearing single acetato bridges in association with isothiocyanato and azido bridges, are found at 1583, 1423  $\text{cm}^{-1}$  ( $\Delta \bar{\nu} = 160 \text{ cm}^{-1}$ ) and 1583, 1417  $\text{cm}^{-1}$  ( $\Delta \bar{\nu} = 166 \text{ cm}^{-1}$ ), respectively. For **3a** two distinct  $\bar{\nu}_{\text{C-N}}$  vibrations appear at 2100 and 2015  $\text{cm}^{-1}$  for the presence of terminal and bridging isothiocyanato ligands.<sup>30</sup> Single  $\bar{\nu}_{\text{C-S}}$  stretching mode appears at 737  $\text{cm}^{-1}$ . For two types of azido ligands in **3b** the  $\bar{\nu}_{\text{as(N}_3)}$  bands appear at 2072 and 2042  $\text{cm}^{-1}$ . While the single weaker  $\bar{\nu}_{\text{s(N}_3)}$  band appears at 1336  $\text{cm}^{-1}$ .<sup>31</sup>

**Assessment for nickel(II) coordination environment.** The electronic spectra of five complexes in MeOH solutions and their solid state diffuse reflectance spectra recorded in 200-800 nm range reveal that the coordination environment around each nickel(II) is roughly either square planar<sup>32</sup> or octahedral<sup>33</sup> (Fig. S2). In MeOH solutions ( $10^{-3}$  M) absorptions bands above 600 nm due to standard *d-d* transitions were hidden by strong charge transfer transitions for all the complexes. However in the solid state the band at 491 nm, can be assigned to the *d-d* transition for square planar  $\text{Ni}^{\text{II}}$  centers in **1**.<sup>34</sup> The solid state diffuse reflectance spectra of **2a-3b** show  ${}^3\text{A}_{2\text{g}}(\text{F}) \rightarrow {}^3\text{T}_{1\text{g}}(\text{P})$  transitions at 614, 623, 617 and 618 nm, respectively. Like solution state measurements here also other two low energy spin-allowed transitions  ${}^3\text{A}_{2\text{g}}(\text{F}) \rightarrow {}^3\text{T}_{1\text{g}}(\text{F})$  and  ${}^3\text{A}_{2\text{g}}(\text{F}) \rightarrow {}^3\text{T}_{2\text{g}}(\text{F})$  were missing.<sup>35</sup> The highly intense bands at 395 nm ( $\epsilon = 5800 \text{ L mol}^{-1} \text{ cm}^{-1}$ ), 391 nm ( $\epsilon = 6500 \text{ L mol}^{-1} \text{ cm}^{-1}$ ), 391 nm ( $\epsilon = 5700 \text{ L mol}^{-1} \text{ cm}^{-1}$ ), 393 nm ( $\epsilon = 6000 \text{ L mol}^{-1} \text{ cm}^{-1}$ ), 397 nm ( $\epsilon = 8600 \text{ L mol}^{-1} \text{ cm}^{-1}$ ) in MeOH and 388, 379, 368, 364 and 388 nm in solid state for **1-3b** may be assigned to ligand-to-metal charge transfer transitions. The absorptions at 254 nm ( $\epsilon = 19900 \text{ L mol}^{-1} \text{ cm}^{-1}$ ), 255 nm ( $\epsilon = 22500 \text{ L mol}^{-1} \text{ cm}^{-1}$ ), 254 nm ( $\epsilon = 18400 \text{ L mol}^{-1} \text{ cm}^{-1}$ ), 256 nm ( $\epsilon = 21500 \text{ L mol}^{-1} \text{ cm}^{-1}$ ), and 253 nm ( $\epsilon = 27500 \text{ L mol}^{-1} \text{ cm}^{-1}$ ) in MeOH and 241, 251, 250, 248 and 251 nm in solid state are dominated by the ligand-centered  $\pi \rightarrow \pi^*$  transitions (Table 2).

**Table 2.** UV–vis spectral data for **1–3b**

Complex	$\lambda_{\max}$ , nm ( $\epsilon$ , L mol <sup>-1</sup> cm <sup>-1</sup> ) in MeOH	$\lambda_{\max}$ , nm ( $\epsilon$ , L mol <sup>-1</sup> cm <sup>-1</sup> ) in solid state
<b>1</b> (ClO <sub>4</sub> ) <sub>2</sub>	395(5800), 254(19900)	491, 388, 241
<b>2a</b> (CF <sub>3</sub> CO <sub>2</sub> )·H <sub>2</sub> O	391(6500), 255(22500)	614, 379, 251
<b>2b</b> (ClO <sub>4</sub> )·C <sub>3</sub> H <sub>7</sub> NO	391(5700), 254(18400)	623, 368, 250
<b>3a</b>	393(6000), 256(21500)	617, 364, 248
<b>3b</b>	397(8600), 253(27500)	618, 388, 251

**Comparison of powder and single crystals.** The powder XRD technique has been nicely utilized to investigate the phase purity of the five complexes and has also been compared with the simulated data, obtained from the single crystal X-ray diffraction data (Cif files) using the CCDC Mercury software. The results have been shown in the Fig. 1, which indicates that the powder XRD pattern of each complex is consistent with its simulated data, though the differences in intensity is attributed to the preferred orientation of the powder samples. Such correlations confirm the phase purity and exactness of the prepared complexes in powdered form with that in single crystal.

**Fig. 1.** Experimental (green) and simulated (brown) PXRD patterns for **1–3b**.

**Thermal stability in the solid state.** Thermal stability of all the five complexes show characteristic patterns in their temperature vs. weight-loss curves as presented in Fig. S3 in Supporting Information. All five complexes show well-defined stepwise

decomposition pattern. Complex **1**, bearing ligand and one hydroxido group, shows a unique type of decomposition path for removal of ligand upon heating showing steep weight loss at  $\sim 284$  °C. Till 800 °C there is no further weight loss and the thermally stable end product corresponds to NiO (calcd.: 10.8%; found: 10.9%). Complexes **2a** and **2b** have similar type of thermogravimetric decomposition pattern. For **2a**, a initial weight loss of 3.8% (calcd.: 3.9%) corresponds to the loss of one lattice and one coordinate water molecules within  $\sim 84$ -120 °C. The second weight loss of 7.5% (calcd.: 7.9%) within  $\sim 120$ -170 °C is due to removal of metal ion bound DMF molecule and the decomposition of the anhydrous complex starts at  $\sim 270$  °C. At 440 °C another step of weight loss takes place most probably towards the formation of NiO. In the case of **2b** the initial weight loss between  $\sim 90$ -170 °C is 10.1% (calcd.: 10.3%) for the removal of coordinated water and DMF molecules and decomposition of ligand starts at  $\sim 280$  °C till 550 °C from where no further weight loss takes place. Complexes **3a** and **3b** have also similar type of TG decomposition pattern. Between  $\sim 154$ -234 °C, **3a** shows a weight loss of 9.65% (calcd.: 10.1%) for the loss of coordinated DMF molecule and further decomposition starts at  $\sim 254$  °C whereas **3b** is stable up to 195 °C and shows degradation after that.

### Establishment of varying coordination environment and Ni...Ni separation

$[\text{Ni}_2(\mu\text{-L})(\mu\text{-OH})](\text{ClO}_4)_2 \cdot \{\text{1}(\text{ClO}_4)_2\}$ . The dicationic fragment  $[\text{Ni}_2(\mu\text{-L})(\mu\text{-OH})]^{2+}$  in  $\text{1}(\text{ClO}_4)_2$ , crystallizing in the monoclinic  $P2_1/n$  space group with  $Z = 4$ , is presented in Fig. 2 and selected structural parameters are summarized in Table S1. In dinuclear ligand environment the rare square planar nickel atoms are coordinated to one imine nitrogen (N1/N3), an amine nitrogen (N2/N4) and bridging phenoxido oxygen (O1) of  $\text{L}^-$  and a hydroxido oxygen atom (O2). The degree of distortion from square planar to tetrahedral geometry has been calculated using the  $\tau_4$  index for four coordinated complexes.<sup>36</sup> The  $\tau_4$  values are 0.07 for Ni1 and 0.06 for Ni2 indicating almost negligible distortion from square planar geometry. The phenoxido and hydroxido bridge-head angles Ni1-O1-Ni2 and Ni2-O2-Ni1 are  $100.3^\circ$  and provides short Ni...Ni separation of 2.897 Å, which is considerably shorter than other reported values for  $\text{Ni}_2$  complexes bearing two metal ion centers in octahedral geometry.<sup>37</sup> Solvent  $\text{H}_2\text{O}$  molecules are also not available for

making these sites octahedral. The Ni–N<sub>amine</sub> distances (1.911–1.984 Å) are longer than the Ni–N<sub>imine</sub> separations (1.831–1.881 Å).

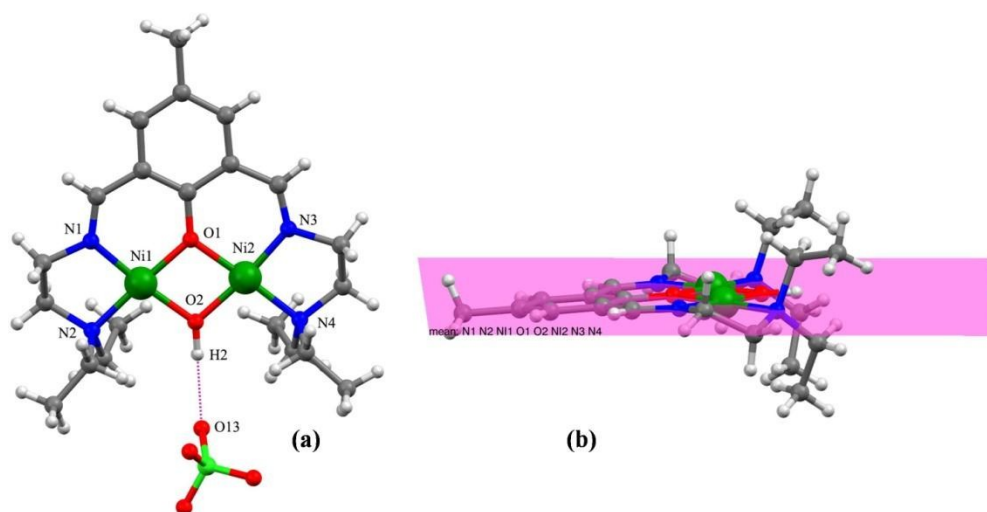


**Fig. 2.** Perspective view of complex **1** and hydrogen bonding interaction with one ClO<sub>4</sub><sup>-</sup> (left). View of complex **1** along the N1, N2, Ni1, O1, O2, Ni2, N3, N4 mean plane (right). Color scheme: Ni, green; O, red; N, blue; C, grey.

The hydroxide H atom (H2) involved in hydrogen bonding with the O13 of one of the lattice perchlorate anion (Table S2), which is responsible for trapping of this anion unavailable for coordination to the metal ions from *apical* sites.

[Ni<sub>2</sub>(μ-L)(μ-CF<sub>3</sub>CO<sub>2</sub>)<sub>2</sub>(C<sub>3</sub>H<sub>7</sub>NO)(H<sub>2</sub>O)](CF<sub>3</sub>CO<sub>2</sub>)·H<sub>2</sub>O {**2a**(CF<sub>3</sub>CO<sub>2</sub>)·H<sub>2</sub>O} and [Ni<sub>2</sub>(μ-L)(μ-CH<sub>3</sub>CH<sub>2</sub>CO<sub>2</sub>)<sub>2</sub>(C<sub>3</sub>H<sub>7</sub>NO)(H<sub>2</sub>O)]ClO<sub>4</sub>·C<sub>3</sub>H<sub>7</sub>NO {**2b**(ClO<sub>4</sub>)·C<sub>3</sub>H<sub>7</sub>NO}. The monocationic fragments **2a**<sup>+</sup> and **2b**<sup>+</sup> crystallize in triclinic  $P\bar{1}$  and monoclinic  $P2_1/n$  space group. Their molecular views are presented in Fig. 3 and selected structural parameters are tabulated in Table S3. Both the complexes are cationic aggregates of two nickel(II) ions linked together by the action of the N<sub>4</sub>O pentadentate ligand L<sup>-</sup> (Scheme 2). The bridging function is accomplished by the central phenoxido group of L<sup>-</sup>, while the imine and amine N atoms at each side of the ligand fulfill two more coordination sites of each nickel(II) center, respectively. Two ancillary carboxylato bridges constitute second and third bridges within the complex *via* O donor atoms. Hexacoordination

around each Ni ion is achieved through binding of water and DMF and introduces asymmetry in distorted octahedral  $N_2O_4$  environment. The phenoxido-bridged Ni-O distances are marginally different in  $2a^+$  (2.048 and 2.078 Å) and in  $2b^+$  (2.050 Å) these are symmetric. Whereas each carboxylato bridge systematically shows one short and one long Ni-O bond to two Ni atoms in both of the complexes. The amine N atoms (2.212-2.250 Å) are further away from nickel(II) than the imine N atoms (1.982-2.010 Å). It may be due to the different N hybridization and also to avoid the steric congestion between the ethyl and bridging carboxylato groups. The intramolecular Ni...Ni distance is 3.475 Å in  $2a^+$  relative to 3.382 Å in  $2b^+$ , which are longest among the three types of complexes presented in this work and indicates that this distance is dependent on the nature of the bridging carboxylato anions.

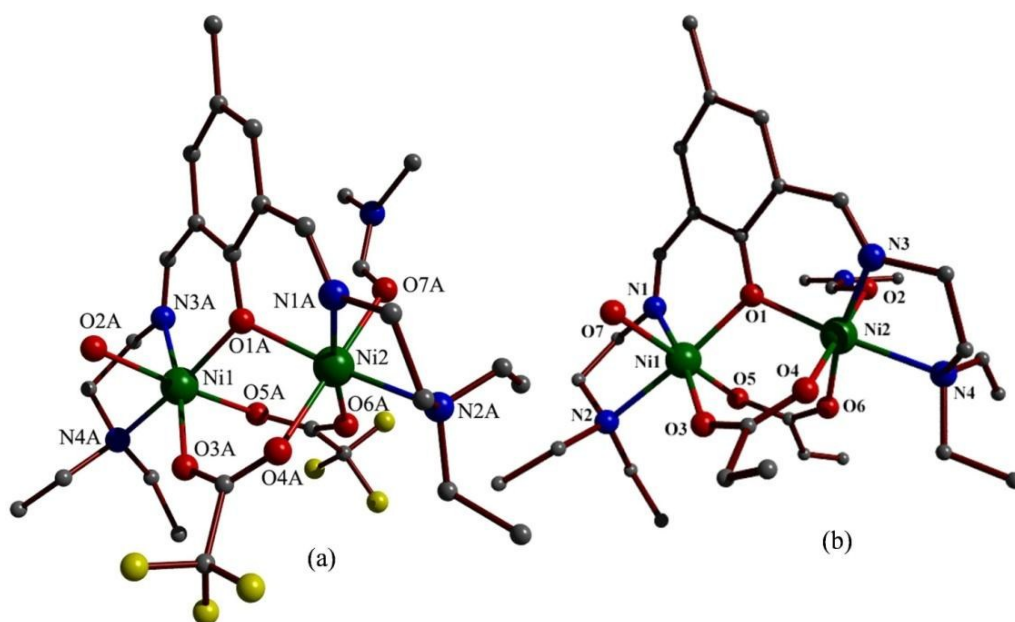


**Fig. 3.** Perspective view of  $2a^+$  (left) and  $2b^+$  (right) with partial atom-numbering scheme. H atoms, anions, and lattice solvent molecules have been omitted for clarity. Color scheme: Ni, green; O, red; N, blue; C, grey and F, yellow.

In  $2a(CF_3CO_2) \cdot H_2O$ , the hydrogen atoms (H22 and H21), attached with O2A of the coordinated water molecule forms strong H-bonds with oxygen atom (O8A) of trifluoroacetate anion and lattice water oxygen atom (O10A) ( $O \cdots O$ , 2.811 and 2.738 Å).

Similarly, hydrogen atoms (H101 and H102) of lattice water molecule involves in H-bonding interaction with trifluoroacetate anion oxygen atoms (O9A and O9A\*) ( $O\cdots O$ , 2.858 and 2.865 Å). Thus, coordinated and lattice water molecules form a hydrogen-bonding network with trifluoroacetate anions as shown in Fig. 4 (Table S4). In case of **2b**(ClO<sub>4</sub>)·C<sub>3</sub>H<sub>7</sub>NO the coordinated water molecule connects the lattice DMF molecule and the perchlorate anion ( $O\cdots O$ , 2.903 and 2.674 Å) through intramolecular hydrogen-bonding interaction (Fig. S4; Table S4).

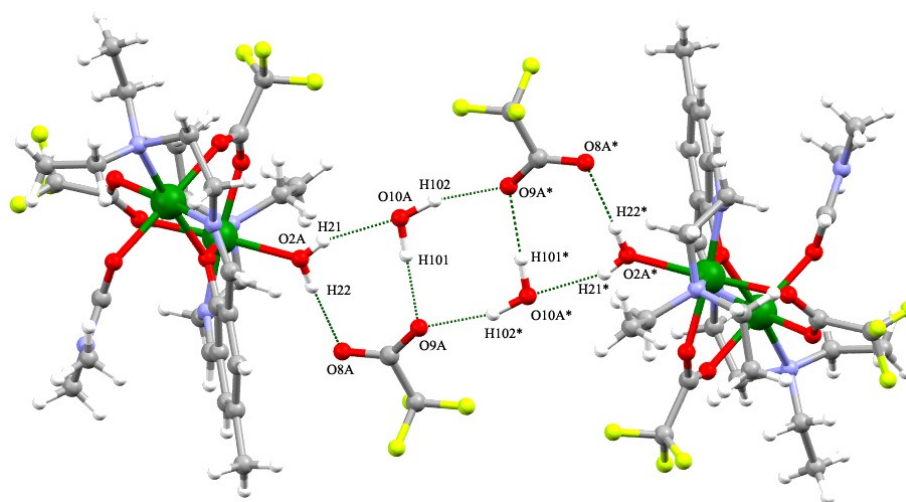


**Fig. 4.** View of hydrogen-bonding network for trapping of anions and solvents in the crystal lattice in **2a**(CF<sub>3</sub>CO<sub>2</sub>)·H<sub>2</sub>O. Color scheme: Ni, green; O, red; N, blue; C, grey and F, yellow.

[Ni<sub>2</sub>(μ-L)(μ-CH<sub>3</sub>CO<sub>2</sub>)(μ-NCS)(NCS)(C<sub>3</sub>H<sub>7</sub>NO)] (**3a**) and [Ni<sub>2</sub>(μ-L)(μ-CH<sub>3</sub>CO<sub>2</sub>)(μ-N<sub>3</sub>)(N<sub>3</sub>)(C<sub>3</sub>H<sub>7</sub>NO)] (**3b**). Complexes **3a** and **3b** crystallize in orthorhombic *Fdd2* and monoclinic *P2<sub>1</sub>/c* space group. Perspective views are presented in Fig. 5 and bond parameters are tabulated in Table S5. Like **2a**<sup>+</sup> and **2b**<sup>+</sup> ligand L<sup>-</sup> bridges two nickel(II) ions through its phenoxido group and the imine and amine N atoms occupy two other coordination positions (Scheme 2). Single isothiocyanato or azido and acetato bridges function as second and third bridges within the complex *via* N and O donor atoms. Electroneutrality and six-coordinate geometry around each Ni ion is obtained through binding of isothiocyanato or azido groups and DMF. The Ni-O distances from phenoxido-bridge are very close in both of the complexes (2.025-2.047 and 2.042-2.052

Å for **3a** and **3b** respectively). N atoms from amine donor groups (2.161-2.209 Å) are further away from nickel(II) than the imine N atoms (1.990-2.003 Å). For single N atom bridges from isothiocyanato and azido groups the intramolecular Ni...Ni distances are 3.074 Å in **3a** and 3.037 Å in **3b**, which are intermediate among the three types of complexes presented in this work.

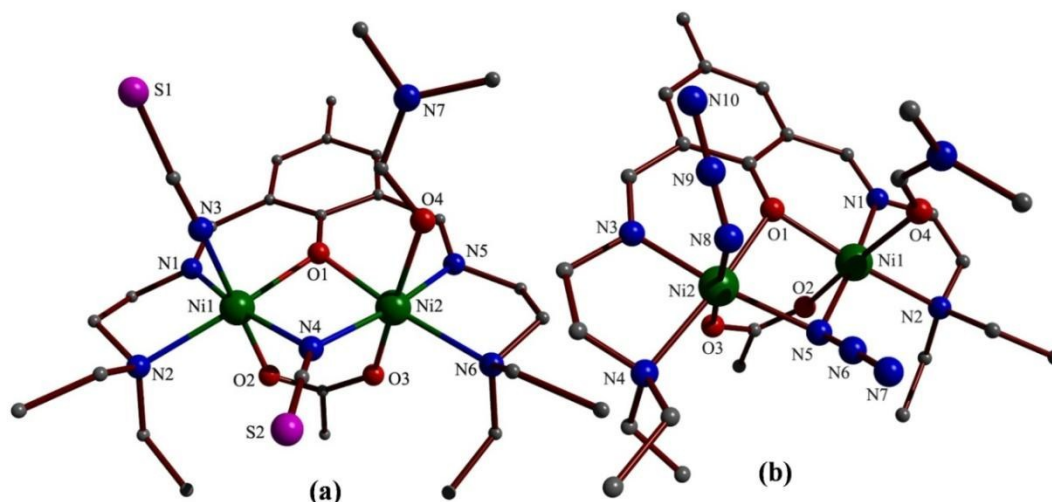


**Fig. 5.** Perspective view of **3a** (left) and **3b** (right) with partial atom-numbering scheme. H atoms are omitted for clarity. Color scheme: Ni, green; O, red; N, blue; C, grey and S, pink

### Hirshfeld surfaces

The analysis using crystal structure data provides a visual picture, where the various types of interactions can be clearly identified by the shapes, contours, and colors provided by the computation and has been generated from CrystalExplorer 3.1.<sup>13</sup> It provided insight into the intermolecular interactions within the molecular crystal. The Hirshfeld surfaces of **1-3b** mapped over  $d_{\text{norm}}$  ( $-0.5$  to  $1.5$  Å) are presented in Fig. 6. The surfaces of **1-3b** mapped over the curvedness ( $-4.0$  to  $0.4$  Å) and shape index ( $-1.0$  to  $1.0$  Å) are displayed in Fig. S5, ESI. The deep red visible spots on the  $d_{\text{norm}}$  surfaces are due to the hydrogen bonding contacts and other visible spots are indicative of H...H contacts. The dominant O...H interactions are viewed as bright red area and C-H...O interactions are as light red spots (Fig. 6). The inside of the bimetallic region in all cases is mainly of

white color and that the surface of the bridging anion has also many white regions which have contacts are around the van der Waals distance.

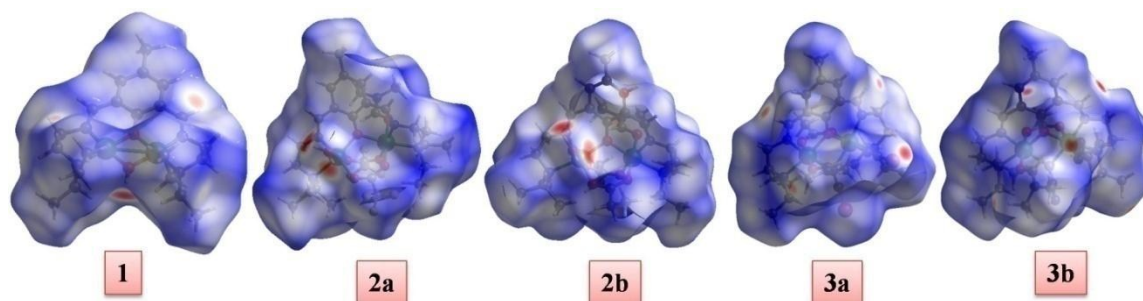


**Fig. 6.** Hirshfeld surfaces mapped over  $d_{\text{norm}}$  for complexes  $[\mathbf{1}(\text{ClO}_4)_2]\text{-}\mathbf{3b}$ .

### HSA binding behavior

Human serum albumin is the major constituent of blood plasma which maintains the osmotic pressure of the blood compartment. HSA have a single tryptophan (Trp-214) residue buried in the second helix of the second domain, in a hydrophobic fold (site 1 of subdomain IIA). One way to measure the extent and accessibility of protein binding sites to transition metal complexes involves fluorescence quenching. The fluorescence from the indole moiety in Trp is extremely sensitive to its environment, and is a convenient spectroscopic probe for the identification of structural changes in the protein and monitoring rotational dynamics surrounding the Trp residue. The interaction of our synthesized complexes with HSA was investigated by monitoring the Trp fluorescence in the titration experiment. The observed fluorescence quenching in the present study is due to the interactions among the dinuclear nickel(II) complexes, Trp-214 residue and its immediate vicinity, which consists of positively charged amino acid residues like Lys-195, Lys-199, Arg-218, Arg-222 and hydrophobic amino acid residues like Phe-211, Leu-238, Ile-264. In general, dinuclear complexes are having substantial advantages in comparison with the corresponding mononuclear complexes as they possess a more no of hydrophobic ligands with greater cationic charge and therefore should bind to HSA with greater affinity. The quenching of fluorescence emission from Trp residue of HSA in absence and presence of **1**, **2a** and **2b** are shown in Fig. 7. The free HSA shows strong Trp fluorescence at 347 nm upon excitation at 295 nm. Upon successive addition of the

three nickel(II) complexes, there occur a significant decrease in Trp fluorescence of HSA. This indicates that cationic nickel(II) complexes can act as quenching agents and diminish the fluorescence of the fluorophore. The used ligand system and the nickel(II) complexes do not show any kind of fluorescence behavior under the used experimental conditions. The Stern–Volmer equation can be used to determine the fluorescence quenching process (eq 8).

$$\frac{F_0}{F} = 1 + K_{SV}[Q] \quad \dots \quad (8)$$

Where  $F_0$  and  $F$  are the unquenched-to-quenched fluorescence intensities in absence and presence of the nickel(II) quencher complexes respectively,  $[Q]$  is the concentration of the quencher and  $K_{SV}$  is the Stern–Volmer constant.  $K_{SV}$  is related to both the fluorescence lifetime of the fluorophore and the rate constant for the quenching process (eq 9).

$$K_{SV} = k_q \tau_0 \quad \dots \quad (9)$$

$k_q$  is the bimolecular quenching constant and  $\tau_0$  is the life time of the unquenched fluorophore (5 ns).<sup>38</sup> The quenching constant, also known as the binding constant  $K_a$  and number of binding sites ( $n$ ) between the protein and metal complexes were calculated using the Scatchard eq 10.<sup>39</sup>

$$\log \frac{F_0 - F}{F} = \log K_a + n \log [Q] \quad \dots \quad (10)$$

The binding constant ( $K_a$ ) for the formation of adducts between the nickel(II) complexes and HSA was determined using the double logarithmic plots (Fig. 7c-f-i). The binding site values ( $n$ ) were determined from the slopes from the use of eq. 10. The  $k_q$  values ( $\sim 10^{13}$ ) of the complexes **1-2b** (Table 4) are higher than the limiting diffusion constants ( $K_{dif} = 2.0 \times 10^{10} \text{ M}^{-1} \text{ s}^{-1}$ ) of biomolecules<sup>40</sup> indicate that static quenching is predominant in these systems.<sup>8b,41</sup> Our *not-so-small* dinuclear nickel(II) complexes are unique in quenching the fluorescence of Trp in HSA *via* a thermodynamically favorable interactions with high binding constant values. The fluorescence quenching by **2a** is the greatest in this group (Table 3, 80%).

**Table 3.** Percent decrease in fluorescence intensity of HSA ( $2.0 \times 10^{-6} \text{ M}$ ) after addition of 23  $\mu\text{M}$  of quencher complexes

Complexes	% decrease
<b>1</b>	69
<b>2a</b>	80
<b>2b</b>	78

The binding constants of the three complexes follow the order **2a** > **2b** > **1** as presented in Table 4. Higher affinity of **2a** and **2b** to HSA than **1** possibly due to better hydrophobic interactions with amino acid residues Phe-211, Leu-238, Ile-264 around Trp-214 probe residue with bridging trifluoroacetate and propionate groups. Table 4 shows a direct relation between the binding constant values and number of binding sites.

**Table 4.** Summary of the Stern-Volmer constant,  $K_{SV}$ , quenching constant,  $k_q$ , binding constant,  $K_a$ , and number of binding sites,  $n$ , for the interactions of three complexes

System	$K_{SV}$ (L mol <sup>-1</sup> )	$k_q$ (L mol <sup>-1</sup> s <sup>-1</sup> )	$K_a$ (L mol <sup>-1</sup> )	$n$
HSA- <b>1</b>	$8.97 \times 10^4$	$1.794 \times 10^{13}$	$4.356 \times 10^4$	1.24
HSA- <b>2a</b>	$16.33 \times 10^4$	$3.266 \times 10^{13}$	$6.133 \times 10^4$	1.37
HSA- <b>2b</b>	$14.26 \times 10^4$	$2.852 \times 10^{13}$	$5.896 \times 10^4$	1.29

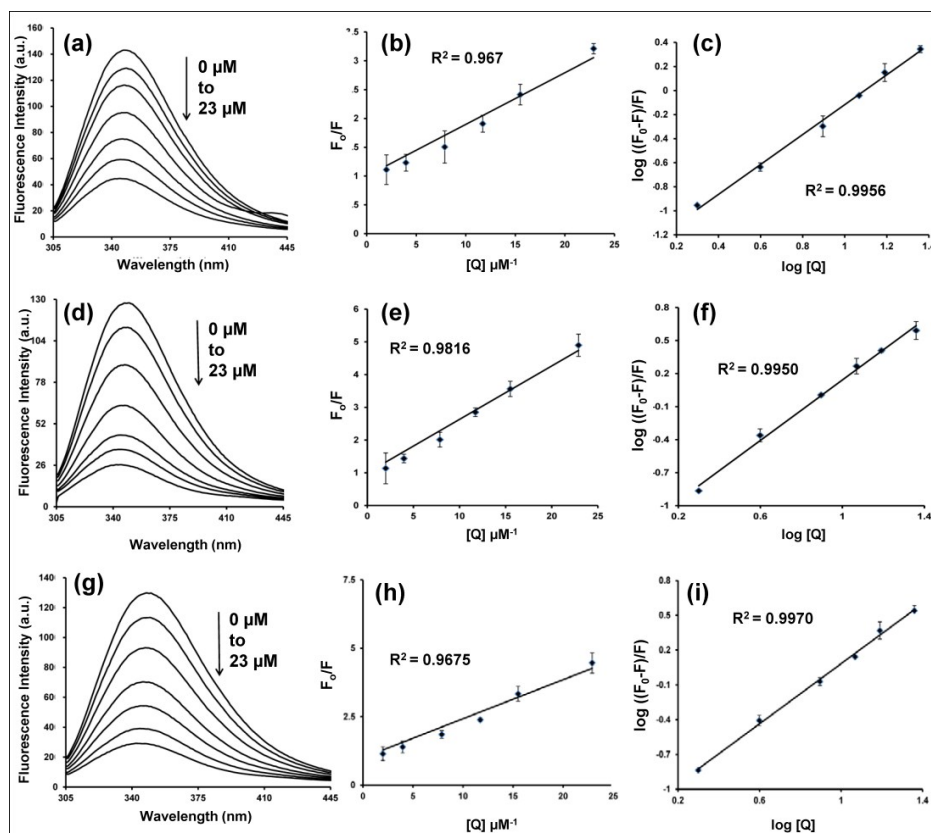


**Fig. 7** (a, d, g) Fluorescence emission spectra of HSA (2  $\mu\text{M}$ ) in absence (top most line) and presence of different concentrations (0 to 23  $\mu\text{M}$ ) of **1**, **2a** and **2b**, respectively, in 10 mM phosphate buffer of pH 7.4 at 298K; (b, e, h) Stern-Volmer and (c, f, i) double logarithmic plots of **1**, **2a** and **2b**, respectively.

### DNA binding aptitude

The DNA binding ability of three cationic complexes **1**, **2a** and **2b** (100  $\mu\text{M}$  in all cases) was studied by performing absorbance (UV-vis) titrations with CT-DNA (0–50  $\mu\text{M}$ ) in 10 mM phosphate buffer at pH 7.4 (Fig. 8). Electronic absorption spectroscopy is frequently used to determine the binding affinity of transition metal complexes with DNA helix. Intercalative mode of binding in between base pairs of DNA usually results in hypochromism (decrease in absorbance). On the other hand, metal complexes binding in non-intercalative fashion or electrostatically with DNA, may result in hyperchromism (increase in absorbance). The magnitude of hypochromism is commonly consistent with the strength of intercalative interaction.<sup>9b,42</sup> In the present study, UV-vis absorption titrations shows a decrease in molar absorptivity for three charged complexes with

increasing concentration of CT-DNA. These spectral characteristics suggest that the binding between complex and DNA is mainly through intercalative interactions in which the flat basic molecular structures assist the complex to intercalate to DNA. The ground state association constant ( $K_a$ ) can be calculated following the Benesi-Hildebrand approach using eq 11.<sup>43</sup>

$$\frac{1}{\Delta A} = \frac{1}{(\varepsilon_b - \varepsilon_f)L_T} + \frac{1}{(\varepsilon_b - \varepsilon_f)L_T K_a} \frac{1}{M} \dots (11)$$

Here  $\varepsilon_b$  and  $\varepsilon_f$  are the extinction coefficients (charge transfer band) of Ni<sub>2</sub> complex in fully bound form and of free complex respectively, for a particular DNA concentration  $M$ .  $L_T$  is the total Ni<sub>2</sub> complex concentration and  $\Delta A$  is the change in the absorbance at a given wavelength. By plotting the reciprocal of  $\Delta A$  versus the reciprocal of concentration of CT-DNA, the association constant ( $K_a$ ) can be obtained from the ratio of the intercept to the slope. All the spectra were corrected by subtracting the spectra of CT-DNA from the Ni<sub>2</sub> complex-CT-DNA spectra. The association constants of the three complexes follow the order **1** > **2a** > **2b** as presented in Table 5.

**Table 5.** Association constants ( $K_a$ ) for the interaction of CT-DNA (0–50  $\mu$ M) with Ni-complexes (100  $\mu$ M) at 298K

System	$K_a$ (L mol <sup>-1</sup> )
CT-DNA- <b>1</b>	$1.358 \pm 0.014 \times 10^5$
CT-DNA- <b>2a</b>	$5.29 \pm 0.51 \times 10^4$
CT-DNA- <b>2b</b>	$4.70 \pm 0.23 \times 10^4$

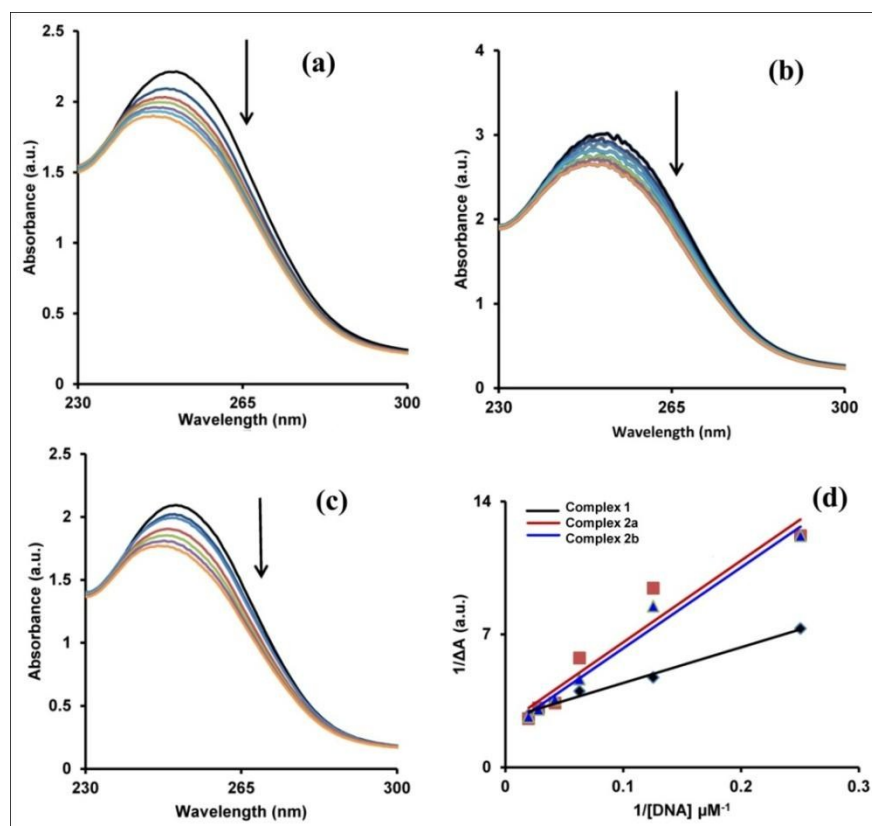


**Fig. 8.** (a to c) Absorption spectra of **1**, **2a** and **2b** (100 μM) in absence (black) and presence (colored) of incremental CT-DNA (0–50 μM) in 10 mM phosphate buffer of pH 7.4; (d) Benesi–Hildebrand double reciprocal plot for these complexes.

Similarly, fluorescence spectral titrations were also performed to study the relative binding affinity of Ni<sub>2</sub> complexes **1**, **2a** and **2b** for CT-DNA. Fluorescent emission of ethidium bromide (EB) is used as optical probe, as no fluorescence is observed for the complexes at room temperature in aqueous solution. EB is a weak fluorescent reagent in water/buffer and belongs to aromatic fluorescent compounds, when it intercalates to DNA, its emission intensity has been enormously enhanced when the system (EB-DNA) is excited at 480 nm. The competitive binding of Ni<sub>2</sub> complex to EB-DNA system leads to generation of free EB, for which the fluorescence intensity of EB in EB-DNA complex decreases. The intensity of EB-DNA complex decreases with gradual addition of Ni<sub>2</sub> complexes due to intercalation (Fig. 9). If EB which has bound to CT-DNA was replaced

by the metal complexes, fluorescence emission intensity of the EB–DNA system will decrease. The modified Stern-Volmer equation (eq 12) can be used to analyze the

$$\frac{F_0}{F_0 - F} = \frac{1}{f_a} + \frac{1}{[Q]} \frac{1}{f_a K_A} \quad \dots (12)$$

fluorescence quenching process, where  $F_0$  and  $F$  are the relative fluorescence intensities in absence and presence of the quencher,  $f_a$  is the fraction of fluorophore accessible to quencher,  $[Q]$  is the concentration of the quencher and  $K_A$  is the modified Stern-Volmer quenching constant. The obtained values of  $K_A$  and  $f_a$  are tabulated in Table 6. The plot of  $F_0/F_0 - F$  versus  $1/[Q]$  (Fig. 9d) yields  $1/f_a$  as the intercept, and  $1/K_A f_a$  as the slope. From the intercept and slope the values for  $f_a$  and  $K_A$  can be obtained.

**Table 6.** Modified Stern-Volmer quenching constants and fraction of fluorophore accessible to quencher complexes at 298K

System	$K_A$ (L mol <sup>-1</sup> )	$f_a$
CT-DNA- <b>1</b>	$4.78 \pm 0.09 \times 10^4$	0.61
CT-DNA- <b>2a</b>	$4.30 \pm 0.20 \times 10^4$	0.71
CT-DNA- <b>2b</b>	$2.25 \pm 0.11 \times 10^4$	0.99

Modified Stern-Volmer quenching constants follow the order **1** > **2a** > **2b**, establishing the fact that the nearly planar complex **1**, having nickel(II) centers in square-planar environment intercalates efficiently with CT-DNA in comparison to the other two complexes (**2a** and **2b**), where nickel(II) ions are in octahedral geometry.

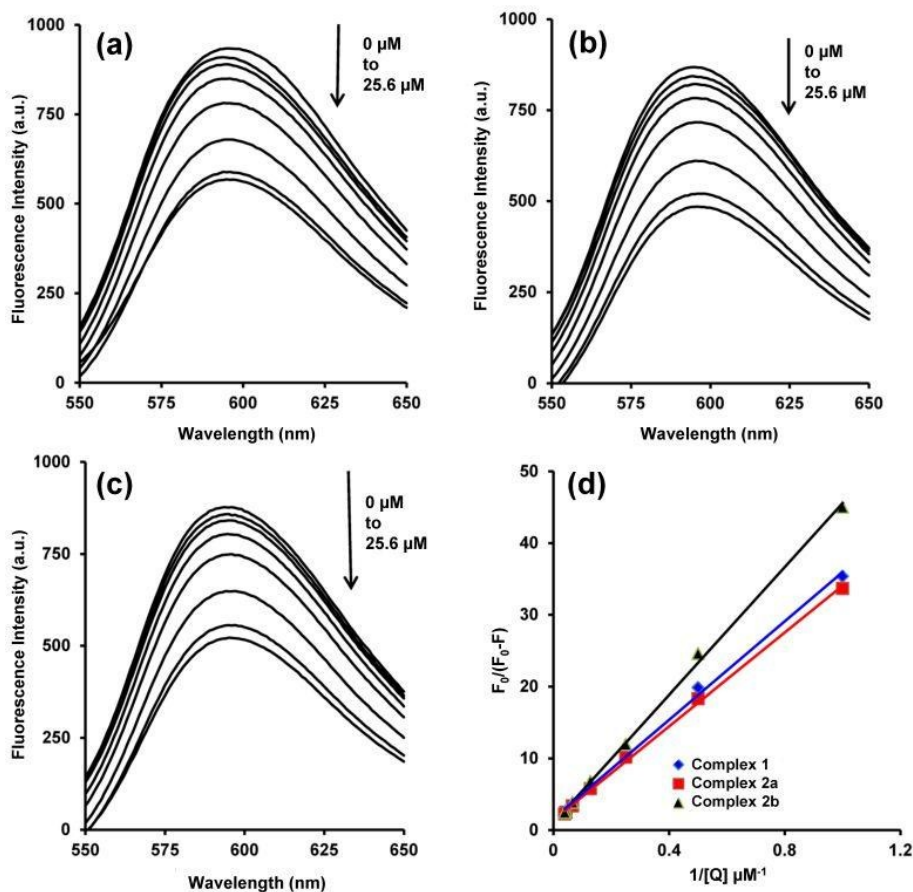


**Fig. 9.** (a to c) Effect of **1**, **2a** and **2b** on the fluorescence emission spectra of EB-DNA system ( $\lambda_{\text{ex}} = 480$  nm);  $C_{\text{EB}} = 5$   $\mu\text{M}$ ;  $C_{\text{DNA}} = 50$   $\mu\text{M}$ ; ranges of concentration for three complexes are from 0 to 25.6  $\mu\text{M}$  at 298K in 10 mM phosphate buffer of pH 7.4. (d) Modified Stern Volmer plot of respective complexes.

## Conclusions

In this work, we have shown that the complexation behavior of the phenolate-based multidentate ligand HL with nickel(II) ions in absence and presence of other ancillary ligands like carboxylates and pseudo-halides lead to five dinuclear nickel(II) complexes of varying co-ligands, coordination geometry and intermetallic separations. The  $\text{NEt}_2$  bearing capping ligand arms did not show any kind of self-aggregation using dinuclear building motifs. Instead trapping of *in situ* generated  $\text{HO}^-$  ion from water in presence of  $\text{NEt}_3$  provided a reactive  $[\text{Ni}_2]$  complex where both the Ni ions are in square planar geometry. Ligand addition reactions on the square planar complex with two carboxylates

of varying R groups provided two new complexes showed that nature of ancillary bridges are crucial in tuning the Ni...Ni separation of the stable final products. Analysis of the obtained five complexes, in relation to the active site of urease, clearly indicates that hydrophobic ligand arms and presence of bridging groups are important for the coordination architecture around the Ni sites and tuning the intermetallic distances. Fluorescence quenching studies with HSA clearly suggests that three cationic complexes (**1-2b**) featuring hydrophobic ligands exhibit strong and favorable interactions in the order **2a** > **2b** > **1**. Static quenching was found to be the predominant form of quenching taking place in these systems providing high binding constants. DNA binding experiments reveal that the intrinsic DNA binding affinity of the complexes depends upon the nearly planar Schiff base ligand functioning as the DNA recognition element. Both UV-vis and fluorescence spectral measurements indicate that complex association follows the order **1** > **2a** > **2b** with the nearly planar complex **1** intercalates efficiently with CT-DNA compared to the other two having metal ions in octahedral geometry. We are currently working to exploit the use of asymmetric ancillary bridges in this reaction system to obtain other *3d-3d* bimetallic complexes.

### Supporting Information

X-ray Crystallographic data in CIF format, Scheme S1, Tables S1–S5 and Figures S1–S5.

### Corresponding Author

\*E-mail: [dray@chem.iitkgp.ernet.in](mailto:dray@chem.iitkgp.ernet.in)

### Notes

The authors declare no competing financial interests.

### Acknowledgements

TSM and SNC are thankful to the University Grant Commission, New Delhi, India for research fellowship. Dr. A. Singha Roy is acknowledged for his help. DST, New Delhi is acknowledged for providing the single crystal X-ray diffractometer facility in the Department of Chemistry, IIT Kharagpur under its FIST program.

### References

1. (a) L. Holm and C. Sander, *Proteins*, 1997, **28**, 72–82; (b) H. L. T. Mobley, M. D. Island and R. P. Hausinger, *Microbiol. Rev.*, 1995, **59**, 451–480; (c) C. Follmer, *Phytochemistry*, 2008, **69**, 18–28.
2. (a) B. Zambelli, F. Musiani, S. Benini and S. Ciurli, *Acc. Chem. Res.*, 2011, **44**, 520–530; (b) P. A. Karplus, M. A. Pearson and R. P. Hausinger, *Acc. Chem. Res.*, 1997, **30**, 330–337.
3. (a) M. A. Halcrow and G. Christou, *Chem. Rev.*, 1994, **94**, 2421–2481; (b) H. E. Wages, K. L. Taft and S. J. Lippard, *Inorg. Chem.*, 1993, **32**, 4985–4987.
4. A. M. Barrios and S. J. Lippard, *J. Am. Chem. Soc.*, 2000, **122**, 9172–9177.
5. M. C. Jimenez, M. A. Miranda and I. Vaya, *J. Am. Chem. Soc.*, 2005, **127**, 10134–10135.
6. (a) J. R. Simard, P. A. Zunszain, J. A. Hamilton and S. Curry, *J. Mol. Biol.*, 2006, **361**, 336–351; (b) S. Fujiwara and T. Amisaki, *Chem. Pharm. Bull.*, 2011, **59**, 860–867.
7. (a) X. M. He and D. C. Carter, *Nature*, 1992, **358**, 209–215; (b) D. C. Carter and X. M. He, *Science*, 1990, **249**, 302–303; (c) D. C. Carter, X. M. He, S. H. Munson, P. D. Twigg, K. M. Gernert, M. B. Broom and T. Y. Miller, *Science*, 1989, **244**, 1195–1198.
8. (a) H. F. Crouse, J. Potoma, F. Nejrabi, D. L. Snyder, B. S. Chohan and S. Basu, *Dalton Trans.*, 2012, **41**, 2720–2731; (b) C. Harford and B. Sarkar, *Acc. Chem. Res.*, 1997, **30**, 123–130; (c) A. Ray, B. K. Seth and U. Pal and S. Basu, *Spectrochim. Acta Part A*, 2012, **92**, 164–174.
9. (a) J. Tan, L. Zhu and B. Wang, *Dalton Trans.*, 2009, 4722–4728; (b) P. Krishnamoorthy, P. Sathyadevi, R. R. Butorac, A. H. Cowley, N. S. P. Bhuvanesh and N. Dharmaraj, *Dalton Trans.*, 2012, **41**, 6842–6854; (c) K. J. Davis, C. Richardson, J. L. Beck, B. M. Knowles, A. Guédin, J.-L. Mergny, A. C. Willis and S. F. Ralph, *Dalton Trans.*, 2015, **44**, 3136–3150; (d) R. Raj Kumar, M. K. Mohamed Subarkhan and R. Ramesh, *RSC Adv.*, 2015, **5**, 46760–46773; (e) R. Prabhakaran, P. Kalaivani, P. Poornima, F. Dallemer, G. Paramaguru, V. Vijaya Padma, R. Renganathan, R. Huang and K. Natarajan, *Dalton Trans.*, 2012, **41**, 9323–9336; (f) S. Anbu, M. Kandaswamy and B. Varghese, *Dalton Trans.*, 2010, **39**, 3823–3832; (g) S. Anbu, S. Shanmugaraju and M. Kandaswamy, *RSC Adv.*, 2012, **2**, 5349–5357; (h) V. K. Bhardwaj and A. Singh, *Inorg. Chem.* 2014, **53**, 10731–10742.

10. (a) F. R. Keene, J. A. Smith and J. G. Collins, *Coord. Chem. Rev.*, 2009, **253**, 2021–2035; (b) W. O. Foye, *Cancer Chemotherapeutic Agents*; American Chemical Society: Washington, DC, 1995; (c) L. H. Hurley, *Nat. Rev. Cancer*, 2002, **2**, 188–200.
11. J. Lorösch, U. Quotschalla and W. Haase, *Inorg. Chim. Acta*, 1987, **131**, 229–236.
12. R. R. Gagne, C. L. Spiro, T. J. Smith, C. A. Hamann, W. R. Thies and A. K. Shiemke, *J. Am. Chem. Soc.*, 1981, **103**, 4073–4081.
13. S. K. Wolff, D. J. Grimwood, J. J. McKinnon, M. J. Turner, D. Jayatilaka, M. A. Spackman, *Crystal Explorer 3.1*; University of Western Australia, 2012.
14. M. E. Reichmann, S. A. Rice, C. A. Thomas and P. Doty, *J. Am. Chem. Soc.*, 1954, **76**, 3047–3053.
15. *Saint, Smart and XPREP*; Siemens Analytical X-ray Instruments Inc.: Madison, WI, 1995.
16. G. M. Sheldrick, *SHELXS-97*, University of Göttingen, Göttingen, Germany, 1997.
17. G. M. Sheldrick, *SHELXL 97, Program for Crystal Structure Refinement*, University of Göttingen, Göttingen, Germany, 1997.
18. *WinGX System*, v. 1.80.05, L. Farrugia, University of Glasgow, UK.
19. G. M. Sheldrick, *SADABS: Software for Empirical Absorption Correction*; University of Göttingen, Institute für Anorganische Chemie der Universität, Göttingen, Germany, 1999–2003.
20. Z. Otwinowski and W. Minor, *Processing of X-ray Diffraction Data Collected in Oscillation Mode, Methods in Enzymology*, vol. 276: *Macromolecular Crystallography*, part A, ed. C. W. Carter, Jr. and R. M. Sweet, Academic Press, New York, 1997, p. 307–326.
21. R. H. Blessing, *Acta Crystallogr., Sect. A* 1995, **51**, 33–37.
22. A. Altomare, M. C. Burla, M. Camalli, G. L. Cascarano, C. Giacovazzo, A. Guagliardi, A. G. G. Moliterni, G. Polidori and R. Spagna, *J. Appl. Crystallogr.*, 1999, **32**, 115–119.
23. M. Nardelli, *J. Appl. Crystallogr.*, 1995, **28**, 659.
24. L. J. Farrugia, *J. Appl. Crystallogr.*, 1999, **32**, 837–838.
25. *DIAMOND, Visual Crystal Structure Information System*, version 3.1; Crystal Impact: Bonn, Germany, 2004.

26. W. J. Geary, *Coord. Chem. Rev.*, 1971, **7**, 81–122.
27. R. J. Hathaway and A. E. Underhill, *J. Chem. Soc.*, 1961, 3091–3096.
28. S. Sarkar, S. Majumder, S. Sasmal, L. Carrella, E. Rentschler and S. Mohanta, *Polyhedron*, 2013, **50**, 270–282.
29. (a) A. Ozarowski, I. B. Szymańska, T. Muzioł and J. Jezierska, *J. Am. Chem. Soc.*, 2009, **131**, 10279–10292. (b) G. Socrates, *Infrared Characteristic Group Frequencies*; Wiley, New York, 1980.
30. (a) K. Nakamoto, *Infrared Spectra of Inorganic and Coordination Compounds*; Wiley Interscience. New York, 1970; p 187; (b) T. Koga, H. Furutachi, T. Nakamura, N. Fukita, M. Ohba, K. Takahashi and H. Ōkawa, *Inorg. Chem.*, 1998, **37**, 989–996.
31. A. Escuer, M. A. S. Goher, F. A. Mautner and R. Vicente, *Inorg. Chem.*, 2000, **39**, 2107–2112.
32. L. K. Das, A. Biswas C. J. Gómez-García, M. G. B. Drew and A. Ghosh, *Inorg. Chem.*, 2014, **53**, 434–445.
33. R. M. Buchanan, M. S. Mashuta, K. J. Oberhausen and J. F. Richardson, *J. Am. Chem. Soc.*, 1989, **111**, 4497–4498.
34. A. Miedaner, R. C. Haltiwanger and D. L. Dubois, *Inorg. Chem.*, 1991, **30**, 417–427.
35. A. K. Ghosh, M. Shatruk, V. Bertolasi, K. Pramanik and D. Ray, *Inorg. Chem.*, 2013, **52**, 13894–13903.
36. L. Yang, D. R. Powell and R. P. Houser, *Dalton Trans.*, 2007, 955–964.
37. (a) A. Biswas, L. K. Das, M. G. B. Drew, G. Aromí, P. Gamez and A. Ghosh, *Inorg. Chem.*, 2012, **51**, 7993–8001; (b) T. Chattopadhyay, M. Mukherjee, A. Mondal, P. Maiti, A. Banerjee, K. S. Banu, S. Bhattacharya, B. Roy, D. J. Chattopadhyay, T. K. Mondal, M. Nethaji, E. Zangrando and D. Das, *Inorg. Chem.*, 2010, **49**, 3121–3129; (c) T. Koga, H. Furutachi, T. Nakamura, N. Fukita, M. Ohba, K. Takahashi and H. Ōkawa, *Inorg. Chem.*, 1998, **37**, 989–996; (d) H. Adams, S. Clunas, D. E. Fenton and S. E. Spey, *J. Chem. Soc. Dalton Trans.*, 2002, 441–448.
38. J. R. Lakowicz, *Principles of Fluorescence Spectroscopy*, third ed., Springer Publishers, New York, 2006.
39. G. Scatchard, *Ann. N. Y. Acad. Sci.*, 1949, **51**, 660–672.

40. M. R. Eftink, *Fluorescence Quenching Reaction: Probing Biological Macromolecular Structures, Biophysical and Biochemical Aspects of Fluorescence Spectroscopy*, Plenum Press, New York, 1991.
41. (a) X.-B. Fu, D.-D. Liu, Y. Lin, W. Hu, Z.-W. Mao and X.-Y. Le, *Dalton Trans.*, 2014, **43**, 8721–8737; (b) C.-Y. Gao, X. Qiao, Z.-Y. Ma, Z.-G. Wang, J. Lu, J.-L. Tian, J.-Y. Xu and S.-P. Yan, *Dalton Trans.*, 2012, **41**, 12220–12232.
42. (a) P. Krishnamoorthy, P. Sathyadevi, R. R. Butorac, A. H. Cowley, N. S. P. Bhuvaneshc and N. Dharmaraj, *Dalton Trans.*, 2012, **41**, 4423–4436; (b) F. Gao, H. Chao, F. Zhou, Y.-X. Yuan, B. Peng and L.-N. Ji, *J. Inorg. Biochem.*, 2006, **100**, 1487–1494.
43. H. A. Benesi and J. H. Hildebrand, *J. Am. Chem. Soc.*, 1949, **71**, 2703–2707.

## Dinuclear Nickel Complexes of Divergent Ni...Ni Separation Showing Ancillary Ligand Addition and Bio-macromolecular Interaction

Tufan Singha Mahapatra,<sup>a</sup> Susmitnarayan Chaudhury,<sup>a</sup> Swagata Dasgupta,<sup>a</sup> Valerio Bertolasi,<sup>b</sup> and Debashis Ray<sup>\*a</sup>

### Text

Reactions of ligand HL with nickel(II) salts produces a family of five [Ni<sub>2</sub>] complexes of varying co-ligands environments and intermetallic separations and show prominent interactions with HSA and CT-DNA.

### Color graphic

